ChemComm

COMMUNICATION

View Article Online
View Journal | View Issue

Check for updates

Cite this: *Chem. Commun.*, 2018, **54**, 6000

Received 13th April 2018,
Accepted 16th May 2018

DOI: 10.1039/c8cc02938e

rsc.li/chemcomm

Paramagnetic nanoemulsions with unified signals for sensitive ^{19}F MRI cell tracking†

Qiaoli Peng,[a] Yu Li,[a] Shaowei Bo,[a] Yaping Yuan,[b] Zhigang Yang,[b] Shizhen Chen,[b] Xin Zhou[b] and Zhong-Xing Jiang*[a]

As a promising cell tracking technology, ^{19}F MRI suffers from low sensitivity. Here, fluorinated nanoemulsions with a unified ^{19}F signal and paramagnetic relaxation enhancement were developed as ^{19}F MRI cellular tracers with high stability, size controllability, biocompatibility, cellular uptake, and dual-modality for sensitive *in vivo* RAW264.7 cell tracking.

In recent years, cell therapy has become very promising in many challenging diseases. In cell therapy, it is of great importance to observe therapeutic cells *in vivo* and obtain information about them, such as where the cells are, in what cellular state, and how many cells in a location of interest.[1] Therefore, tracking cells *in vivo* with an imaging technology in a real time, non-invasive and quantitative way is highly valuable for elucidating cell functions, monitoring pathological processes, and developing effective cell therapy strategies.[2]

Among the imaging technologies for cell tracking,[1,2] fluorine-19 magnetic resonance imaging (^{19}F MRI) is very attractive because it provides highly selective and quantitative images without ionizing radiation, tissue depth limit, and background signals.[3] For these reasons, ^{19}F MRI has already been applied *in vivo* to monitor a variety of cells in recent years.[4] However, compared to nuclear imaging and optical imaging, the sensitivity of ^{19}F MRI is pretty low. Actually, it remains a formidable challenge to sensitively track cells *in vivo* with ^{19}F MRI. First, a local effective fluorine concentration of at least 10 mM is usually required to generate ^{19}F MRI images.[5] Here, effective fluorines are not the fluorines in a ^{19}F MRI agent but the portion of fluorines which generate the ^{19}F NMR signal for ^{19}F MRI. Second, the non-symmetric allocation of fluorines and the resulting complex ^{19}F NMR signals for most ^{19}F MRI agents dramatically reduce the effective fluorines for ^{19}F MRI and introduce imaging artifacts.[3,6,7] Third, relatively long relaxation times of most ^{19}F MRI agents dramatically prolong the ^{19}F MRI data collection time, which in turn reduces the ^{19}F MRI sensitivity. For these reasons, a high dose of imaging agents or fluorine labelled cells and a long data collection time are usually required to generate *in vivo* ^{19}F MRI cellular images. Therefore, it is essential to develop sensitive ^{19}F MRI cellular tracers by addressing these issues.

Herein, we report fluorinated nanoemulsions with unified ^{19}F NMR signals, paramagnetic relaxation enhancement (PRE), and high stability, biocompatibility and cellular uptake as sensitive ^{19}F MRI-fluorescent dual-modality cellular tracers (Fig. 1). To unify the ^{19}F NMR signals, all 27 fluorines in ^{19}F MRI agent **1** are symmetrically located.[6] To reduce the relaxation times through the PRE-effect, a fluorinated chelator with a high fluorous solubility and paramagnetic ion chelation ability is required. Recently, Ahrens *et al.* developed a perfluoropropyl substituted diketone as a paramagnetic

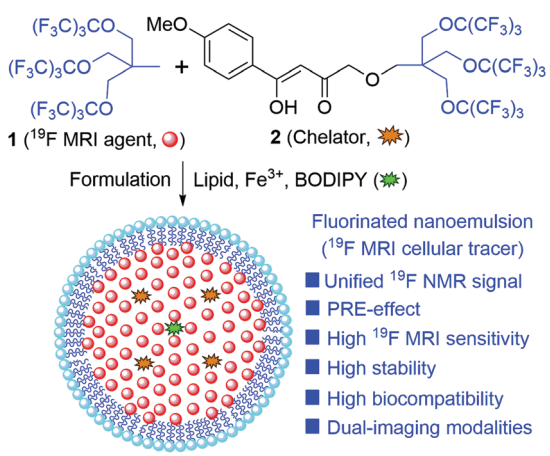

Fig. 1 Design of a nanoemulsion as a ^{19}F MRI cellular tracer.

[a] *Hubei Province Engineering and Technology Research Center for Fluorinated Pharmaceuticals and School of Pharmaceutical Sciences, Wuhan University, Wuhan 430071, China. E-mail: zxjiang@whu.edu.cn*

[b] *State Key Laboratory for Magnetic Resonance and Atomic and Molecular Physics, Wuhan Institute of Physics and Mathematics, Chinese Academy of Sciences, Wuhan 430071, China*

† Electronic supplementary information (ESI) available: ^{19}F NMR of a mixture of **1** and **2**, emulsion stability study, quantification of the ^{19}F concentration in emulsions, the PRE-effect in emulsions, cell viability assays and uptake assessment, ^{19}F MRI procedures, synthesis and characterization of compounds, and copies of spectra. See DOI: 10.1039/c8cc02938e

ion chelator.[7] However, it introduced many non-effective fluorines and complicated the ^{19}F MRI process. It is also noteworthy that effective fluorines only account for 70.7% of all fluorines in this case.[7] So, fluorinated chelator **2** with the same fluorinated moiety and ^{19}F NMR signal as ^{19}F MRI agent **1** was designed. By these means, the effective fluorines are maximized, and the data collection time is shortened, and therefore the ^{19}F MRI sensitivity dramatically improved. In addition to ^{19}F MRI, fluorescence imaging is incorporated into the tracer by encapsulating fluorescent dye BODIPY in the nanoemulsion.

^{19}F MRI agent **1** and chelator **2** were then synthesized in a convenient and scalable way (Scheme 1). Agent **1** was prepared as a clear liquid on a 32.5 g scale through the Mitsunobu ether formation between trimethylolethane **3** and perfluoro-*tert*-butanol.[8] Chelator **2** was prepared as a pale wax in 4 steps from pentaerythritol **4** with Claisen condensation between ester **7** and 4-acetylanisole as the key step. Agent **1** and chelator **2** are insoluble in water due to their high fluorine content. As expected, chelator **2** was soluble in agent **1** and the resulting solution gave a unified ^{19}F NMR peak at −71.3 ppm (Fig. S1, ESI†).

Formulation of fluorinated nanoemulsions was explored on a series of surfactants and additives (Table 1). Lecithin was identified as the surfactant of choice after a few initial formulations. Safflower oil was the additive of choice for formulating ^{19}F MRI agent **1** as **Eml-1**. When a mixture of agent **1** and chelator **2** was formulated, Pluronic F68 provided highly stable **Eml-2** with a smaller PDI than safflower oil (Fig. S2, ESI†). The particle size of **Eml-2** was further manipulated by passing through a cell disrupter, which provided highly stable **Eml-3** with a smaller particle size of 67 nm (Fig. S2, ESI†). To incorporate the PRE-effect and

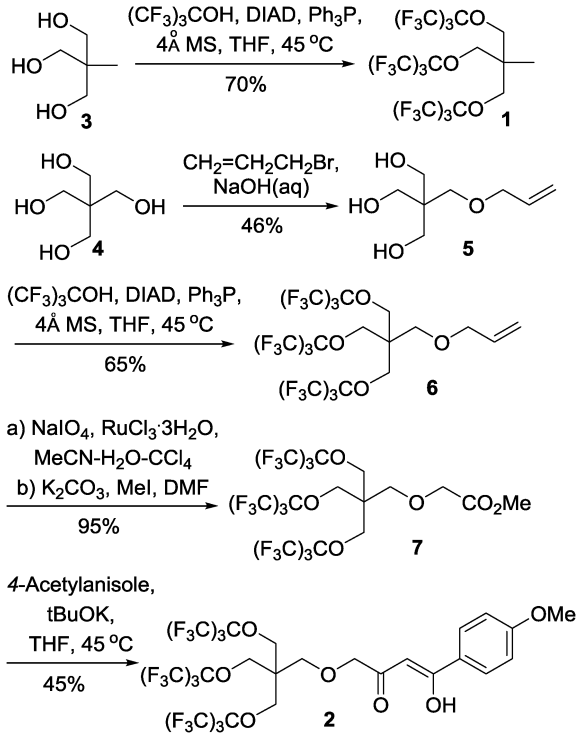

Scheme 1 Synthesis of ^{19}F MRI agent **1** and chelator **2**.

Table 1 Formulation of fluorinated emulsions

Emulsion	Formulation ingredients[a]	Size (PDI)[b]
Eml-1	**1**, lecithin, safflower oil	158 (0.19)
Eml-2	**1**, **2**, lecithin, F68	165 (0.16)
Eml-3[c]	**1**, **2**, lecithin, F68	67 (0.25)
Eml-4	**1**, **2**, lecithin, F68, Fe^{3+}	187 (0.18)
Eml-5	**1**, **2**, lecithin, F68, BODIPY	181 (0.19)
Eml-6	**1**, **2**, lecithin, F68, BODIPY, Fe^{3+}	195 (0.22)

[a] Formulation by stirring the ingredients (77 mg of **1**, 5 mg of **2**, 4% lecithin, 4% safflower oil, 1% F68, and 1 mL of water) for 3 h, then repeating 3 times the process of 10 min ultrasound bath treatment and 1 h stirring. [b] Measured by dynamic light scattering (DLS). [c] Treated with a cell disrupter at 1500 bar 3 times.

fluorescence image into the emulsion, **Eml-4**, **Eml-5**, and **Eml-6** (entries 4–6) carrying paramagnetic Fe^{3+} ions and fluorescent dye BODIPY were then formulated in the presence of lecithin and F68, respectively.

The PRE-effects of many paramagnetic ions were then employed to modulate the longitudinal and transverse relaxation times (T_1 and T_2) of the fluorinated nanoemulsions. With diamagnetic Ga^{3+} as a control, addition of paramagnetic ions Eu^{3+}, Gd^{3+}, Er^{3+}, Tb^{3+}, and Mn^{2+} to **Eml-2** resulted in a slight T_1 reduction and a significant T_2 reduction, respectively (Fig. 2a and b). However, short T_1 and sharp ^{19}F NMR peaks are usually preferred for reducing the ^{19}F MRI scan time and simplifying the ^{19}F MRI procedures.[9] Fortunately, addition of Fe^{3+} to **Eml-2** resulted in significant T_1 and T_2 reductions and a sharp ^{19}F NMR peak because a coordinatively saturated and high-spin Fe^{3+} complex is formed.[7] Similar results were also obtained for **Eml-3** (Fig. S3, ESI†). Fe^{3+}-T_1/T_2 titration experiments on **Eml-1** and **Eml-2** showed that the PRE-effect solely originated from chelated-Fe^{3+} in the nanoparticles (Fig. 2c and d): (1) Significant T_1/T_2 reductions were observed for the ^{19}F signal of **Eml-2**. (2) Little T_1/T_2 reduction was observed in **Eml-1** formulated without chelator **2**. The chelation-induced diffusion of Fe^{3+} in the **Eml-2** solution from the solvent into the nanoparticles was observed through

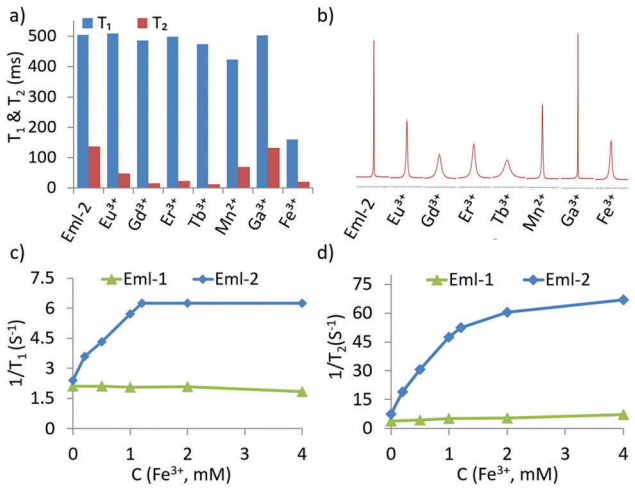

Fig. 2 PRE-effect of 1 mM ions on the ^{19}F relaxation times (a) and peaks (b) of **Eml-2** and Fe^{3+}-T_1/T_2 titration experiments on **Eml-1** and **Eml-2** (c: T_1; d: T_2) at 376 MHz.

the color changes: when the Fe^{3+} concentration was increased, the color of **Eml-2** became dark orange, while the color of **Eml-1** remained light yellow. As highly fluorinated chelator **2** is insoluble in water, dark orange is the color of Fe^{3+}-chelated **2**. A maximum PRE-effect on **Eml-2** was observed at an Fe^{3+}/chelator ratio of about 1 : 3 when all the chelator in the emulsion was chelated with Fe^{3+} (**Eml-4**). A competitive chelation experiment showed a color change from dark orange to light yellow and T_1/T_2 increases when EDTA was added to **Eml-4** solution (Fig. S5, ESI†), which illustrated a reversed diffusion of Fe^{3+} from the nanoparticles to the solvent in the presence of a strong chelator. It was also found that higher temperature promoted the PRE-effect by further shortening T_1 without broadening the ^{19}F NMR peak (Fig. S6, ESI†). Therefore, with chelator **2** in the nanoparticles, paramagnetic Fe^{3+} was efficiently incorporated into the nanoparticles and induced significant T_1 reductions without broadening the ^{19}F NMR peak through its PRE-effects.

The ^{19}F MRI sensitivities of the fluorinated nanoemulsions were then evaluated using *in vitro* ^{19}F MRI experiments. First, the ^{19}F density MRI of **Eml-2** and **Eml-4**, in which the signal intensity (SI) is mostly dependent on the effective ^{19}F concentration in the sample, showed that ^{19}F MRI images were obtained at a low ^{19}F concentration of 8 mM with a data collection time of 64 seconds, respectively (Fig. 3a and Fig. S8, ESI†). In terms of ^{19}F MRI sensitivity, **Eml-2** and **Eml-4** with unified ^{19}F NMR signals showed much higher sensitivity than their peers.[4,5] The SI of ^{19}F MRI is proportional to the ^{19}F concentration, which would be important for a downstream quantitative study (Fig. 3b). Compared to **Eml-2**, quantitative T_1-weighted ^{19}F MRI (brighter image for shorter T_1) and T_2-weighted ^{19}F MRI (darker image for shorter T_2) of **Eml-4** exhibited PRE-induced signal intensity improvements of 61% and 83% at 9.4 T, respectively (Fig. 3c). So, incorporating Fe^{3+} into the nanoemulsion through chelator **2** is an effective strategy to improve the ^{19}F MRI sensitivity.

^{19}F MRI-fluorescence dual-imaging nanoemulsions **Eml-5** and **Eml-6** were then studied. Incorporation of a fluorinated BODIPY resulted in slightly larger nanoparticles in **Eml-5** and **Eml-6**. Similar properties to those of **Eml-2** and **Eml-4**, including the PRE-effect of Fe^{3+}, ^{19}F MRI sensitivity, temperature-promoted PRE-effect, and signal intensity–^{19}F concentration relationship,

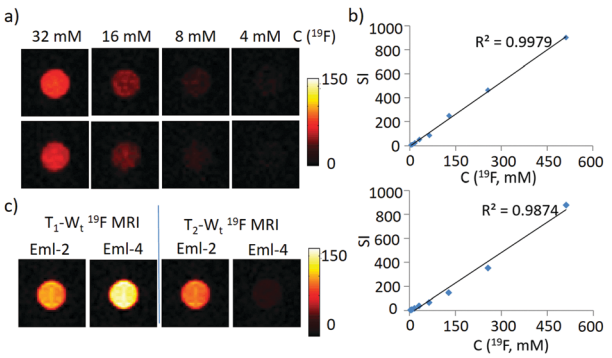

Fig. 3 ^{19}F density MRI of **Eml-2** (a, upper) and **Eml-4** (a, lower), SI *versus* C(^{19}F) of **Eml-2** (b, upper) and **Eml-4** (b, lower), and ^{19}F T_1/T_2-wt MRI of **Eml-2** and **Eml-4** (c, C(^{19}F) = 128 mM) at 9.4 T.

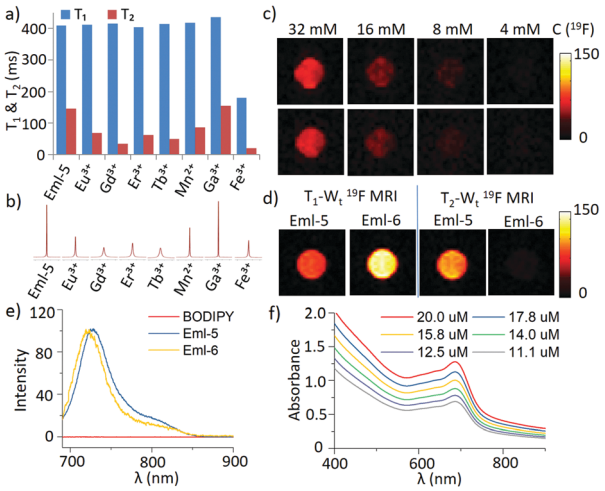

Fig. 4 PRE-effect on the ^{19}F NMR relaxation times (a) and peaks (b) of **Eml-5** at 376 MHz, ^{19}F density MRI (c, upper: **Eml-5**; lower: **Eml-6**) and ^{19}F T_1/T_2-wt MRI (d, C(^{19}F) = 128 mM) at 9.4 T, fluorescence emission (e, C_{BODIPY} = 200 μM) of **Eml-5**, **6**, and concentration-dependent UV absorption of **Eml-6** (f, BODIPY concentrations are indicated).

were also observed for **Eml-5** and **Eml-6** (Fig. 4a–d, Fig. S6 and S8, ESI†). Notably, the Fe^{3+}-induced PRE of **Eml-6** resulted in 82% and 89% improvements of T_1 and T_2-weighted ^{19}F MRI at 9.4 T, respectively. Both emulsions **Eml-5** and **Eml-6** showed sharp fluorescence emission at 725 nm and 727 nm, respectively, and concentration-dependent UV absorption for fluorescence imaging (Fig. 4e and f).

Cytotoxicity assay of the nanoemulsions on human lung adenocarcinoma cells (A549 cells, Fig. 5a), mouse leukemic monocyte–macrophage cells (RAW264.7 cells, Fig. 5b), and mouse fibroblast cells (L929 cells, Fig. S7, ESI†) indicated good biocompatibility of these emulsions. These emulsions can be efficiently taken up by RAW264.7 cells, A549 cells, and L929 cells (Fig. 5c, S7 ESI†). Confocal laser scanning microscopy of

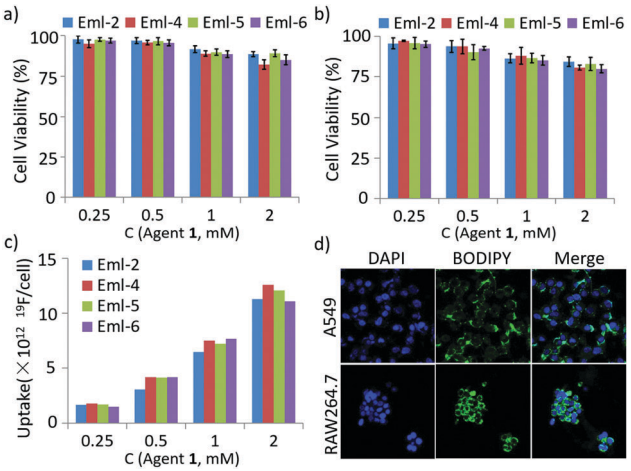

Fig. 5 Cytotoxicity assay of emulsions (**Eml-2**, **Eml-4**, **Eml-5**, **Eml-6**) on A549 cells (a) and RAW264.7 cells (b), RAW264.7 cell uptake of the emulsions (c, 19 h of incubation), and confocal laser scanning microscopy of **Eml-6** treated A549 cells and RAW264.7 cells (d).

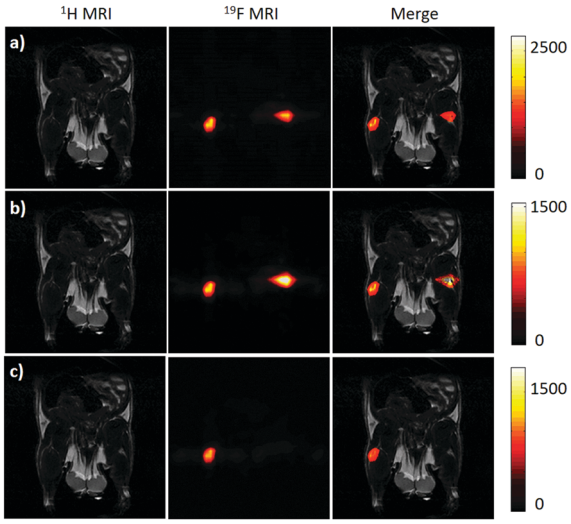

Fig. 6 *In vivo* ^{19}F MRI tracking of **Eml-2** and **Eml-4** labeled RAW264.7 cells in mice (a, ^{19}F density MRI; b, T_1-weighted ^{19}F MRI; c, T_2-weighted ^{19}F MRI, the left side injected with **Eml-2** labeled cells, the right side injected with **Eml-4** labeled cells).

Eml-6 treated A549 cells and RAW264.7 cells confirmed that **Eml-6** can be taken up by these cells.

Finally, a proof of concept study of *in vivo* ^{19}F MRI RAW264.7 cell tracking in Balb/c nude mice was carried out. After labeling RAW264.7 cells with **Eml-2** and **Eml-4**, 6×10^6 cells were subcutaneously injected into the left and right hind regions of a mouse, respectively. After 24 h, ^{19}F density MRI clearly showed both regions with comparable intensities due to the comparable ^{19}F concentrations (Fig. 6a). More importantly, because of the PRE-effect in **Eml-4**-labeled cells, T_1 and T_2-weighted ^{19}F MRI indicated signal intensity improvements of 75% and 81%, respectively, in the **Eml-4**-labeled cell region as compared to the **Eml-2**-labeled cell region. So, **Eml-4** would be a sensitive ^{19}F MRI *in vivo* cellular tracer.

In summary, we have developed a series of fluorinated nanoemulsions with controllable particle sizes and multi-functionality for highly sensitive ^{19}F MRI cell tracking. As a long journey to ^{19}F MRI-guided cell therapy, the sensitivity issue of ^{19}F MRI dramatically limited its clinical applications. Compared to existing ^{19}F MRI cellular tracers, the ^{19}F MRI sensitivities of fluorinated nanoemulsions here are improved by both the unified ^{19}F signal and paramagnetic relaxation enhancement of Fe^{3+}. With easily available components and convenient formulation, these fluorinated nanoemulsions can be employed as versatile platforms for cell tracking, such as ^{19}F MRI-fluorescence dual-imaging tracers and microenvironment-responsive ^{19}F MRI tracers, and in cell imaging-traceable drug release systems, *etc.* With such promising fluorinated nanoemulsions, ^{19}F MRI may increasingly play crucial roles in elucidating the cell therapy mechanism, optimizing therapeutic strategies, and beyond.

We are thankful for financial support from the National Key Research and Development Program of China (2016YFC1304704), the National Natural Science Foundation of China (21402144 and 21572168), the Major Project of Technology Innovation Program of Hubei Province (2016ACA126), and the State Key Laboratory of Magnetic Resonance and Atomic and Molecular Physics (Wuhan Institute of Physics and Mathematics).

Conflicts of interest

There are no conflicts to declare.

Notes and references

1 (*a*) A. T. Chan and M. R. Abraham, *J. Nucl. Cardiol.*, 2012, **19**, 118; (*b*) E. T. Ahrens and J. W. M. Bulte, *Nat. Rev. Immunol.*, 2013, **13**, 755; (*c*) D. M. Kurtz and S. S. Gambhir, *Adv. Cancer Res.*, 2014, **124**, 257; (*d*) N. G. Kooreman, J. D. Ransohoff and J. C. Wu, *Nat. Mater.*, 2014, **13**, 106.
2 (*a*) M. Srinivas, A. Heerschap, E. T. Ahrens, C. G. Figdor and I. J. M. de Vries, *Trends Biotechnol.*, 2010, **28**, 363; (*b*) A. Taylor, K. M. Wilson, P. Murray, D. G. Fernig and R. Levy, *Chem. Soc. Rev.*, 2012, **41**, 2707; (*c*) Y. Wang, C. Xu and H. Ow, *Theranostics*, 2013, **3**, 544; (*d*) M. P. Alcolea and P. H. Jones, *Nat. Rev. Cancer*, 2013, **13**, 167; (*e*) R. Meir, M. Motiei and R. Popovtzer, *Nanomedicine*, 2014, **9**, 2059; (*f*) P. K. Nguyen, J. Riegler and J. C. Wu, *Cell Stem Cell*, 2014, **14**, 431; (*g*) W. W.-W. Hsiao, Y. Y. Hui, P.-C. Tsai and H.-C. Chang, *Acc. Chem. Res.*, 2016, **49**, 400.
3 (*a*) J. Ruiz-Cabello, B. P. Barnett, P. A. Bottomley and J. W. M. Bulte, *NMR Biomed.*, 2011, **24**, 114; (*b*) J. C. Knight, P. G. Edwards and S. J. Paisey, *RSC Adv.*, 2011, **1**, 1415; (*c*) I. Tirotta, V. Dichiarante, C. Pigliacelli, G. Cavallo, G. Terraneo, F. B. Bombelli, P. Metrangolo and G. Resnati, *Chem. Rev.*, 2015, **115**, 1106.
4 (*a*) E. T. Ahrens, R. Flores, H. Xu and P. A. Morel, *Nat. Biotechnol.*, 2005, **23**, 983; (*b*) J. M. Janjic, M. Srinivas, D. K. K. Kadayakkara and E. T. Ahrens, *J. Am. Chem. Soc.*, 2008, **130**, 2832; (*c*) M. Srinivas, P. Boehm-Sturm, C. G. Figdor, I. J. de Vries and M. Hoehn, *Biomaterials*, 2012, **33**, 8830; (*d*) C. Gonzales, H. A. I. Yoshihara, N. Dilek, J. Leignadier, M. Irving, P. Mieville, L. Helm, O. Michielin and J. Schwitter, *PLoS One*, 2016, **11**, e0164557; (*e*) J. M. Gaudet, A. M. Hamilton, Y. Chen, M. S. Fox and P. J. Foster, *Magn. Reson. Med.*, 2017, **78**, 713.
5 I. Tirotta, A. Mastropietro, C. Cordiglieri, L. Gazzera, F. Baggi, G. Baselli, M. G. Bruzzone, I. Zucca, G. Cavallo, G. Terraneo, F. B. Bombelli, P. Metrangolo and G. Resnati, *J. Am. Chem. Soc.*, 2014, **136**, 8524.
6 (*a*) Z.-X. Jiang, X. Liu, E.-K. Jeong and Y. B. Yu, *Angew. Chem., Int. Ed.*, 2009, **48**, 4755; (*b*) S. Bo, C. Song, Y. Li, W. Yu, S. Chen, X. Zhou, Z. Yang, X. Zheng and Z.-X. Jiang, *J. Org. Chem.*, 2015, **80**, 6360; (*c*) W. Yu, Y. Yang, S. Bo, Y. Li, S. Chen, Z. Yang, X. Zheng, Z.-X. Jiang and X. Zhou, *J. Org. Chem.*, 2015, **80**, 4443; (*d*) X. Liu, Y. Yuan, S. Bo, Y. Li, Z. Yang, X. Zhou, S. Chen and Z.-X. Jiang, *Eur. J. Org. Chem.*, 2017, 4461.
7 A. A. Kislukhin, H. Xu, S. R. Adams, K. H. Narsinh, R. Y. Tsien and E. T. Ahrens, *Nat. Mater.*, 2016, **15**, 662.
8 Z.-X. Jiang and Y. B. Yu, *Tetrahedron*, 2007, **63**, 3982.
9 (*a*) F. Schmid, C. Holtke, D. Parker and C. Faber, *Magn. Reson. Med.*, 2013, **69**, 1056; (*b*) E. De Luca, P. Harvey, K. H. Chalmers, A. Mishra, P. K. Senanayake, J. I. Wilson, M. Botta, M. Fekete, A. M. Blamire and D. Parker, *J. Biol. Inorg. Chem.*, 2014, **19**, 215.